https://doi.org/10.5194/egusphere-2026-2994
Preprint. Discussion started: 17 June 2026
© Author(s) 2026. CC BY 4.0 License.

Latitudinal Variation of Ionospheric Total Electron Content During the 17 March 2015 Geomagnetic Storm: A Multi-Station GNSS Analysis

Nouhaila Bouhadi[1], Toufik Mzili[2], and Hamid Nebdi[1]

[1]Laboratory of Innovation in Science, Technology and Modeling (LISTM), Faculty of Sciences, Chouaib Doukkali University, El Jadida, Morocco
[2]Laboratory LAROSERI, Faculty of Sciences, Chouaib Doukkali University, El Jadida, Morocco

Correspondence: Nouhaila Bouhadi (nouhaila.b137@ucd.ac.ma)

Abstract. We investigated the latitude-dependent ionospheric response to the St. Patrick's Day geomagnetic storm of 17 March 2015 (Dst = -234 nT, Kp = 8) using GNSS-derived vertical total electron content (VTEC) from four stations spanning mid- to auroral latitudes (34–70° N) in the European–African sector: RABT (Rabat, Morocco), MADR (Madrid, Spain), BRUX (Brussels, Belgium), and TRO1 (Tromsø, Norway). VTEC was derived from dual-frequency pseudorange measurements with differential code bias corrections. Storm-time VTEC responses showed clear latitude-dependent variability. Relative enhancements ranged from +46 % at TRO1 to +224 % at BRUX, while the absolute peak VTEC decreased systematically with latitude. Linear regression of peak storm-time VTEC against geographic latitude yielded a gradient of -1.61 ± 0.06 TECU per degree ($R^2 = 0.9968$, $p = 0.001578$). Correlation analysis revealed statistically significant positive associations between hourly ΔVTEC and Kp at RABT and MADR, while BRUX showed a weaker positive but non-significant correlation under the adopted $p < 0.01$ criterion. These results quantify the latitudinal structuring of storm-time ionospheric variability in the European–African sector and highlight stronger positive responses at the mid-latitude stations than at auroral latitude during this event.

1 Introduction

Geomagnetic storms represent one of the principal sources of short-term ionospheric variability, because they modify the electrodynamic and thermospheric conditions controlling the distribution of ionospheric plasma. Such perturbations affect GNSS positioning, radio propagation, and communication systems, making storm-time TEC variability an important quantity for regional space-weather studies (Buonsanto, 1999). One of the most widely used parameters for quantifying ionospheric electron content is the vertical total electron content (VTEC), which provides an integrated measure of ionospheric plasma density and its response to geomagnetic forcing. Among extreme space weather events, the St. Patrick's Day geomagnetic storm of 17 March 2015 stands out as one of the strongest storms of Solar Cycle 24. Triggered by a fast Earth-directed coronal mass ejection (Wu et al., 2016), this event produced intense geomagnetic activity (Astafyeva et al., 2015; Jacobsen and Andalsvik, 2016). The storm generated pronounced ionospheric disturbances on a global scale, providing a valuable opportunity to investigate the cou-

https://doi.org/10.5194/egusphere-2026-2994
Preprint. Discussion started: 17 June 2026
© Author(s) 2026. CC BY 4.0 License.

pling between the magnetosphere, thermosphere, and ionosphere under extreme conditions. Previous studies of the March 2015 storm have demonstrated diverse regional responses. In particular, Astafyeva et al. reported strong positive ionospheric storms at mid-latitudes, with TEC enhancements exceeding 200%, while Cherniak and Zakharenkova (2016) documented storm-time plasma-density depletion structures extending into the European mid-latitude sector. Nava et al. (2016) showed that storm-time VTEC responses depend strongly on latitude, local time, and longitude, reflecting the interplay between prompt penetration electric fields (PPEFs), disturbance dynamo electric fields (DDEFs), neutral wind dynamics, and auroral energy deposition. In the African and European longitude sector, latitudinal features of TEC during the St. Patrick's Day storm were further documented by Paul et al. (2018), highlighting marked regional contrasts in storm-time ionospheric behaviour. Additional analyses of the 17 March 2015 event over the European–African sector also revealed multiple ionospheric perturbations and strong spatial variability in TEC during storm-time conditions (Borries et al., 2016; Akala et al., 2023; Habyarimana et al., 2023). Other studies have likewise confirmed the strong spatial and temporal variability of storm-time ionospheric disturbances using GNSS and multi-instrument approaches (Astafyeva et al., 2017; Berényi et al., 2023; Mošna et al., 2024). The physical drivers of storm-time TEC disturbances are not uniform across latitude. At low and middle latitudes, rapid electric-field penetration from the magnetosphere can modify the vertical plasma drift and produce short-timescale TEC enhancements, particularly during the storm sudden commencement and main phase (Kelley, 2009; Huang et al., 2005). Several hours later, storm-induced neutral winds can generate disturbance dynamo electric fields, which may counteract the earlier penetration-field effects and contribute to delayed or negative ionospheric responses (Blanc and Richmond, 1980; Fejer and Scherliess, 1997). At auroral latitudes, the response is more strongly controlled by particle precipitation, Joule heating, and composition changes. These processes can reduce the O/N_2 ratio and therefore lower ionization efficiency, favouring negative storm effects under disturbed conditions (Prölss, 1995; Burns et al., 2004). This strong latitudinal contrast in storm-time response mechanisms highlights the need for coordinated multi-station studies spanning a broad range of latitudes. Although the St. Patrick's Day storm of 17 March 2015 has been extensively documented, previous studies have mainly emphasized global responses, isolated regional sectors, or specific ionospheric manifestations, leaving the storm-time VTEC response in the European–African sector insufficiently constrained as an integrated latitudinal system. In contrast, the present work examines this sector as a coherent station transect within a unified statistical framework combining quiet-day baseline removal, storm-time enhancement analysis, regression of peak VTEC versus latitude, correlation with geomagnetic indices, and time-lagged response assessment. This framework allows us to quantify both the intensity and the spatio-temporal structure of the ionospheric response during the event.

In this study, we investigate the ionospheric response to the March 2015 storm over the European–African sector using GNSS observations from four stations spanning mid- to auroral latitudes (34–70° N). VTEC is derived from high-rate dual-frequency GNSS measurements and analysed together with geomagnetic indices in order to quantify storm-time variability from three complementary perspectives: temporal evolution, latitudinal structuring, and ionosphere–magnetosphere coupling. Specifically, we examine storm-time perturbations relative to quiet-day hourly baselines, derive the latitudinal gradient of peak storm-time VTEC, assess correlations with geomagnetic activity indices, and evaluate delayed responses through time-lag analysis. Independent validation against CODE Global Ionosphere Maps (GIMs) is also performed to assess the robustness of the GNSS-derived VTEC estimates under both quiet and disturbed conditions.

https://doi.org/10.5194/egusphere-2026-2994
Preprint. Discussion started: 17 June 2026
© Author(s) 2026. CC BY 4.0 License.

The objectives of this work are to:

- characterize the temporal evolution of VTEC during the storm across different latitudinal regimes;
- quantify storm-time VTEC perturbations relative to quiet-day hourly baselines;
- determine the latitudinal dependence of peak storm-time ionospheric response;
- assess ionosphere–magnetosphere coupling through correlation and time-lag analyses;
- provide a sector-specific framework for interpreting latitude-dependent storm-time ionospheric variability.

By combining high-resolution GNSS observations with statistical and time-lagged analyses, this study provides a sector-specific assessment of storm-time ionospheric variability during one of the strongest geomagnetic events of Solar Cycle 24.

2 Data sources

2.1 GNSS observations

GNSS observation and navigation files were obtained from the International GNSS Service (IGS) archive (https://www.unavco.org) for the period 15–19 March 2015. GNSS–based TEC and VTEC estimation approaches similar to those employed in the present study have been used in previous ionospheric monitoring and validation studies, including regional GPS–TEC analyses and ESA Space Weather Pilot Project technical reports (Jodogne et al., 2004; Warnant et al., 2003; Nebdi et al., 2004). The study focuses on the geomagnetic storm of 17 March 2015. During this event, the disturbance storm time (Dst) index reached a minimum value of approximately $-234\,\mathrm{nT}$, while the planetary Kp index attained values up to 8, indicating severe geomagnetic activity (Astafyeva et al., 2015). Based on geomagnetic conditions, the study period was divided into three distinct phases:

- **Pre–storm period (15–16 March):** relatively quiet to weakly disturbed geomagnetic conditions preceding the main storm phase, generally characterized by $\mathrm{Kp} < 3$ and $\mathrm{Dst} > -20\,\mathrm{nT}$;
- **Main phase (17 March, 06:00–22:00 UTC):** rapid decrease in Dst;
- **Recovery phase (18–19 March):** gradual recovery of the ring current.

This temporal segmentation allows us to distinguish background ionospheric behaviour from storm-induced perturbations and to place the main storm response within its pre-storm and recovery-phase context. To provide a latitudinal transect spanning mid- to auroral latitudes, four permanent IGS stations were selected: RABT (Rabat, Morocco), MADR (Madrid, Spain), BRUX (Brussels, Belgium), and TRO1 (Tromsø, Norway). These stations ensure coverage across distinct ionospheric regimes, from mid–latitude to auroral regions. Table 1 summarises the station characteristics, including geographic and geomagnetic coordinates and the typical number of tracked satellites. Figure 1 illustrates the geographic distribution of these stations.

https://doi.org/10.5194/egusphere-2026-2994
Preprint. Discussion started: 17 June 2026
© Author(s) 2026. CC BY 4.0 License.

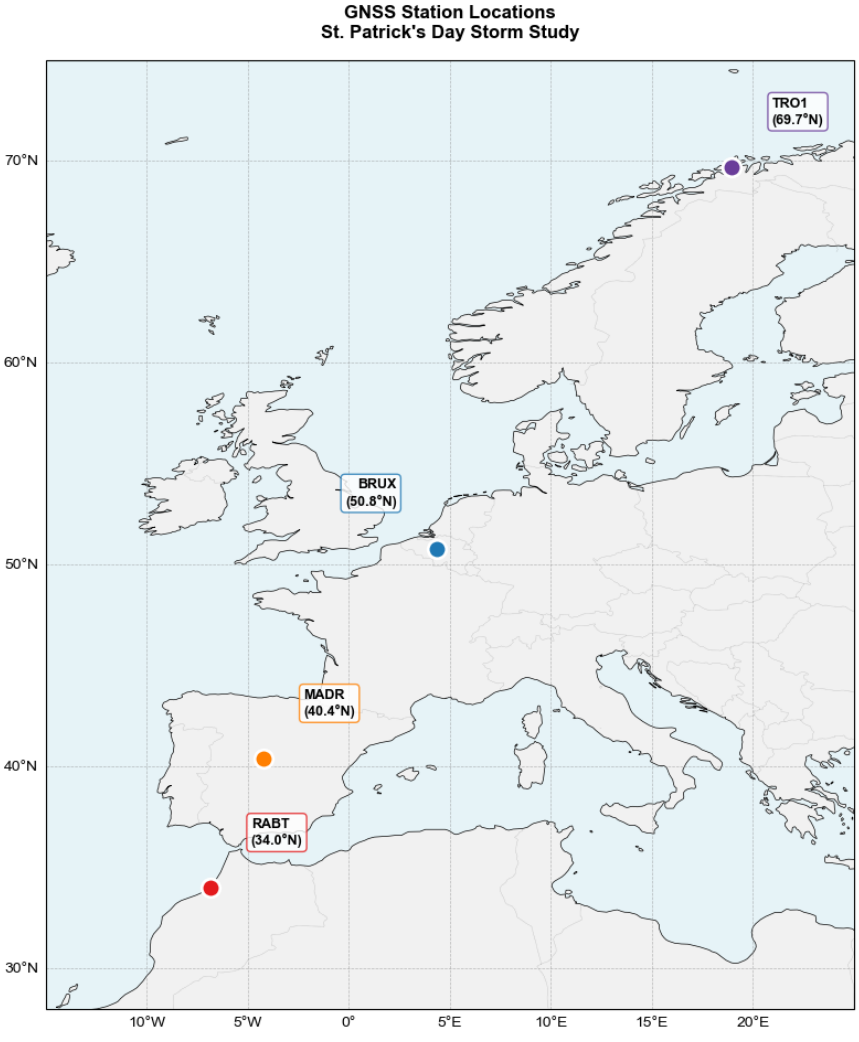

Figure 1. Geographic distribution of GNSS stations used in this study. Stations span 34–70° N (RABT to TRO1), providing latitudinal coverage from mid-latitude through auroral ionospheric regimes. Background map data are from Natural Earth.

2.2 Geomagnetic indices

To quantify global geomagnetic activity and its interaction with the ionosphere, standard geomagnetic indices were used. The planetary Kp index, provided at a 3–hour temporal resolution, was obtained from the GFZ Helmholtz Centre for Geosciences (https://kp.gfz.de). The Dst index, representing the intensity of the magnetospheric ring current, was obtained at 1–hour resolution from the World Data Center for Geomagnetism, Kyoto (https://wdc.kugi.kyoto-u.ac.jp/). These indices were used to identify storm phases and to investigate correlations between geomagnetic activity and ionospheric TEC variability. Previous studies from the same research framework have also investigated geomagnetic activity using K-index-based analyses and pre-

https://doi.org/10.5194/egusphere-2026-2994
Preprint. Discussion started: 17 June 2026
© Author(s) 2026. CC BY 4.0 License.

Table 1. Geographic and geomagnetic characteristics of the GNSS stations used in this study.

ID	City	Country	Geographic Coordinates		Geomagnetic	Satellite
			Latitude	Longitude	Latitude	Count
RABT	Rabat	Morocco	34.0°N	6.9°W	41.2°N	8–12
MADR	Madrid	Spain	40.4°N	3.7°W	46.4°N	9–13
BRUX	Brussels	Belgium	50.8°N	4.4°E	54.1°N	6–10
TRO1	Tromsø	Norway	69.7°N	18.9°E	66.8°N	5–9

dictive approaches. In particular, Nebdi (2010) analysed geomagnetic activity over three solar cycles using a K-index database, while more recent works by Chafik et al. (2024a, b) applied machine-learning and long-term analysis approaches to geomagnetic activity indices.

3 Data processing

3.1 Dual-frequency pseudorange method

We derived Slant Total Electron Content (STEC) from dual–frequency GPS pseudorange observations following standard formulations (Schaer, 1999; Hofmann-Wellenhof et al., 1992). The pseudorange observation equation between a GPS satellite s and a receiver r at frequency f is given by:

$$P_r^s(f) = \rho_r^s + c \cdot b_r(f) - c \cdot b^s(f) + I_r^s(f) + T_r^s + \varepsilon_r^s(f), \tag{1}$$

where

- ρ_r^s is the geometric satellite–receiver distance,
- b_r and b^s represent receiver and satellite clock offsets and hardware delays,
- $I_r^s(f)$ is the ionospheric delay,
- T_r^s is the tropospheric delay,
- $\varepsilon_r^s(f)$ denotes measurement noise and multipath effects.

The ionospheric delay is frequency dependent and proportional to TEC:

$$I(f) = \frac{K}{f^2} \cdot \mathrm{TEC}, \tag{2}$$

https://doi.org/10.5194/egusphere-2026-2994
Preprint. Discussion started: 17 June 2026
© Author(s) 2026. CC BY 4.0 License.

where $K = 40.3\ \mathrm{m^3\,s^{-2}}$, f is the signal frequency in Hz, and TEC is expressed in electrons/m^2 (1 TECU = 10^{16} electrons/m^2). By forming the geometry–free combination of pseudorange observations at two frequencies (f_1 and f_2), geometric, clock, and tropospheric terms are eliminated:

$$P_r^s(f_1) - P_r^s(f_2) = K \cdot \mathrm{STEC}\left(\frac{1}{f_1^2} - \frac{1}{f_2^2}\right) + \Delta b_r - \Delta b^s + \varepsilon, \tag{3}$$

where Δb_r and Δb^s are the differential code biases (DCB) of the receiver and satellite, respectively. For satellite elevation angles above $10°$, the noise term ε is assumed to be negligible. DCB corrections were obtained from the Center for Orbit Determination in Europe (CODE) using daily IONEX files, available at (`ftp://ftp.aiub.unibe.ch/CODE/`). These corrections were applied prior to STEC estimation.

3.2 STEC to VTEC conversion

To remove geometric effects, STEC was converted to Vertical Total Electron Content (VTEC) using a single–layer ionospheric model (Schaer, 1999), in which the ionosphere is assumed to be concentrated in a thin spherical shell at a height of $h = 350$ km above the Earth's surface. Satellite elevation angles E, computed from broadcast ephemerides (Navstar GPS Joint Program Office, 2000) via Earth–Centered Earth–Fixed (ECEF) to East–North–Up (ENU) coordinate transformation, were restricted to $E \geq 30°$ in order to reduce mapping–function amplification, multipath effects, and uncertainties associated with horizontal ionospheric gradients at the ionospheric pierce points.

The mapping function relating STEC to VTEC is defined as:

$$M(\varepsilon) = \frac{1}{\sqrt{1 - \left(\frac{R_e \cos E}{R_e + h}\right)^2}}, \tag{4}$$

where $R_e = 6371$ km is the mean Earth radius. VTEC is then obtained as:

$$\mathrm{VTEC} = \mathrm{STEC}\sqrt{1 - \left(\frac{R_e \cos E}{R_e + h}\right)^2}. \tag{5}$$

3.3 Station-level VTEC computation and temporal resampling

At each 30–second epoch, VTEC values from all valid satellites were averaged:

$$\mathrm{VTEC}_{\mathrm{station}}(t) = \frac{1}{N(t)} \sum_{i=1}^{N(t)} \mathrm{VTEC}_i(t), \tag{6}$$

where $N(t)$ is the number of valid satellites (typically 8–12 at RABT, 9–13 at MADR, 6–10 at BRUX, and 5–9 at TRO1). Epochs with $N(t) < 4$ were excluded. For comparison with geomagnetic indices, the 30-second station-level VTEC series was resampled to hourly means. Dst values were used at their native 1-hour cadence. Because Kp is provided at 3-hour resolution, each Kp value was assigned to the corresponding 3-hour interval when constructing paired hourly ΔVTEC–Kp datasets. The same resampling and pairing procedure was applied independently to all stations.

https://doi.org/10.5194/egusphere-2026-2994
Preprint. Discussion started: 17 June 2026
© Author(s) 2026. CC BY 4.0 License.

3.4 Baseline removal and ΔVTEC calculation

Storm–induced perturbations in vertical total electron content (VTEC) were quantified relative to a quiet–time baseline. A quiet reference day (15 March 2015) was selected based on low geomagnetic activity ($Kp < 3$, $|\mathrm{Dst}| < 20$ nT). For each hour h (0–23 UTC), the hourly baseline VTEC was calculated as the median of all VTEC measurements recorded at that hour on the quiet day. The median was adopted to reduce the influence of residual outliers related to multipath effects, satellite geometry, and short-term ionospheric variability. The hourly baseline is therefore defined as:

$$\mathrm{Baseline}(h) = \mathrm{median}\big[\mathrm{VTEC}(\text{15 March}, h)\big]. \tag{7}$$

Storm–time deviations (ΔVTEC) were then obtained by subtracting the quiet baseline from the observed VTEC,

$$\Delta\mathrm{VTEC}(t) = \mathrm{VTEC}(t) - \mathrm{Baseline}\big(\mathrm{hour}(t)\big), \tag{8}$$

such that positive ΔVTEC indicates enhancement relative to quiet conditions, while negative values indicate ionospheric depletion.

3.5 Statistical analysis

Pearson correlation coefficients between ΔVTEC and the geomagnetic indices were calculated using hourly values. The correlation coefficient was defined as

$$r(\Delta\mathrm{VTEC}, K_p) = \frac{\mathrm{cov}(\Delta\mathrm{VTEC}, K_p)}{\sigma_{\Delta\mathrm{VTEC}} \cdot \sigma_{K_p}}, \tag{9}$$

with an analogous formulation for $-\mathrm{Dst}$, which was used as a proxy for storm intensity. For the Pearson correlations, statistical significance was assessed using $p < 0.01$.

To account for delayed ionospheric responses, time-lagged cross-correlation analysis was performed between hourly ΔVTEC and Kp for lags ranging from -12 to $+12$ hours. Prior to cross-correlation, both series were high-pass filtered using a 24-hour centred rolling-mean subtraction in order to remove slow recovery trends and isolate storm-time variability.

To ensure a consistent inter-station comparison, peak values were extracted using the same storm-time selection criterion for all stations. The latitudinal dependence of the storm-time ionospheric response was quantified by linear regression of the peak hourly mean VTEC values at the four stations against geographic latitude:

$$\mathrm{VTEC}_{\max} = \beta_0 + \beta_1 \phi_{\mathrm{geo}}, \tag{10}$$

where ϕ_{geo} is the geographic latitude, β_0 is the intercept, and β_1 is the latitudinal gradient in TECU per degree. Model performance was assessed using the coefficient of determination (R^2) and the associated p-value.

https://doi.org/10.5194/egusphere-2026-2994
Preprint. Discussion started: 17 June 2026
© Author(s) 2026. CC BY 4.0 License.

3.6 Validation with global ionosphere maps

Previous studies have compared GPS-derived TEC with independent ionosonde-derived TEC estimates and empirical ionospheric models (Jodogne et al., 2004; Warnant et al., 2003). In the present study, GNSS-derived VTEC estimates were validated against Global Ionosphere Maps (GIMs) produced by the Center for Orbit Determination in Europe (CODE). CODE GIMs provide global TEC with a temporal resolution of 2 hours (12 maps per day at even UTC hours: 00, 02, . . . , 22) and a spatial resolution of $5^\circ \times 2.5^\circ$ in longitude and latitude, respectively, representing the ionosphere as a single layer at 450 km altitude (Schaer et al., 1998; Hernández-Pajares et al., 2009). GIMs VTEC values at each station location were obtained from IONEX–format files via bilinear interpolation of the four surrounding grid points. Hourly GNSS–derived VTEC measurements were temporally matched to the nearest GIMs epoch within a 1–hour tolerance. Agreement between the two datasets was quantified using Pearson correlation coefficient (r), root–mean–square error (RMSE), mean absolute error (MAE), and mean bias (GNSS − GIMs). This validation was applied independently to all stations under both quiet and storm conditions to assess the consistency of GNSS–derived VTEC estimates.

4 Results and discussion

4.1 Validation against CODE Global Ionosphere Maps

The VTEC values derived from GNSS were compared with CODE global ionospheric maps (GIMs) to assess their consistency during the period from 15 to 19 March 2015. Figure 2 shows time-series comparisons between hourly GNSS-derived VTEC and interpolated GIM VTEC for the four stations over the same period. The hourly GNSS-derived VTEC values were matched to the nearest GIM epoch within a tolerance of one hour, and the agreement was quantified using Pearson's correlation coefficient and standard error statistics (Table 2). At TRO1, the near equality between the MAE and the absolute bias indicates that GNSS-derived VTEC is systematically lower than the corresponding GIM estimate over most matched epochs, rather than fluctuating symmetrically around it. The correlation coefficients range from 0.80 to 0.93, with RMSE values between 5.8 and 8.1 TECU, which correspond to the typical uncertainties of GIMs under disturbed conditions (Hernández-Pajares et al., 2009). The negative bias observed at TRO1 may reflect both a systematic offset between GNSS-derived and GIM-derived VTEC at high latitude and the reduced reliability of global ionospheric maps in auroral regions, where gradients and localized disturbances are particularly strong. Despite systematic offsets at certain stations, particularly at high latitude, the temporal evolution of VTEC is well reproduced, supporting the use of GNSS-derived VTEC for subsequent storm-time analysis (Fig. 3).

4.2 Temporal evolution of VTEC during the storm

During the quiet period on 15 March, all stations exhibit regular diurnal variations in VTEC, with daytime maxima increasing toward lower latitudes (Figs. 4 and 5).

https://doi.org/10.5194/egusphere-2026-2994
Preprint. Discussion started: 17 June 2026
© Author(s) 2026. CC BY 4.0 License.

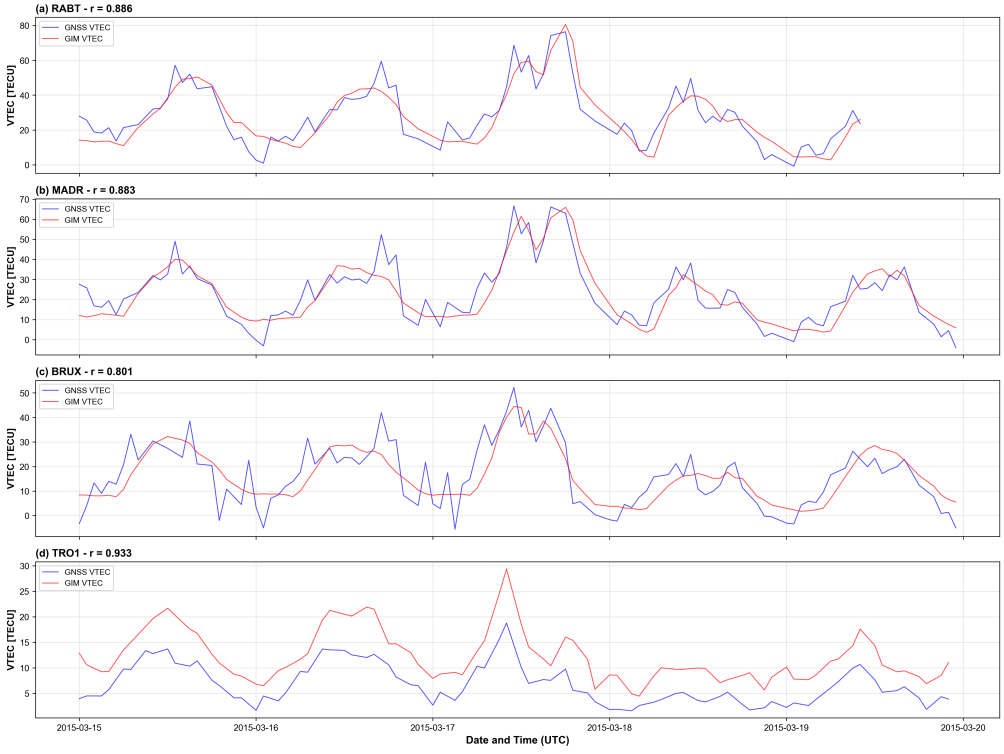

Figure 2. Time series comparison of GNSS–derived VTEC (blue) and CODE GIMs VTEC (red) for (a) RABT, (b) MADR, (c) BRUX, and (d) TRO1 during 15–19 March 2015.

Table 2. Validation statistics for GNSS–derived VTEC against CODE GIMs (15–19 March 2015).

Station	n	r	R^2	RMSE (TECU)	MAE (TECU)	Bias (TECU)
RABT	89	0.886	0.785	8.06	6.62	+0.90
MADR	100	0.883	0.780	7.28	5.95	+0.57
BRUX	104	0.802	0.642	7.59	6.29	+0.29
TRO1	80	0.933	0.871	5.82	5.49	−5.49

n is the number of hourly GNSS–GIMs data pairs; r is the Pearson correlation coefficient; RMSE is the root–mean–square error; MAE is the mean absolute error; Bias is the mean difference (GNSS − GIMs). Positive bias indicates that GNSS–derived VTEC exceeds GIMs values.

https://doi.org/10.5194/egusphere-2026-2994
Preprint. Discussion started: 17 June 2026
© Author(s) 2026. CC BY 4.0 License.

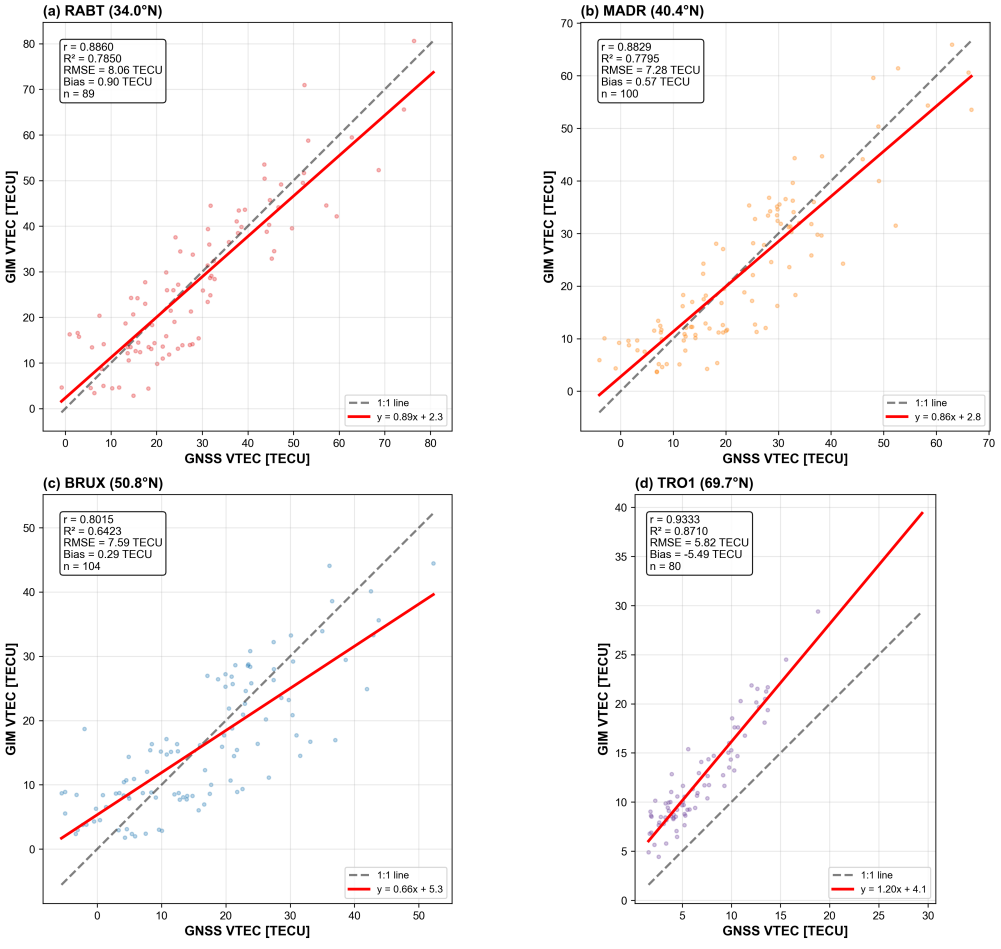

Figure 3. Scatter plots comparing hourly GNSS–derived VTEC and CODE GIMs VTEC for (a) RABT, (b) MADR, (c) BRUX, and (d) TRO1 during 15–19 March 2015. The dashed line represents the 1:1 relationship, while solid red lines show linear regression fits. Statistical metrics are indicated in each panel.

https://doi.org/10.5194/egusphere-2026-2994
Preprint. Discussion started: 17 June 2026
© Author(s) 2026. CC BY 4.0 License.

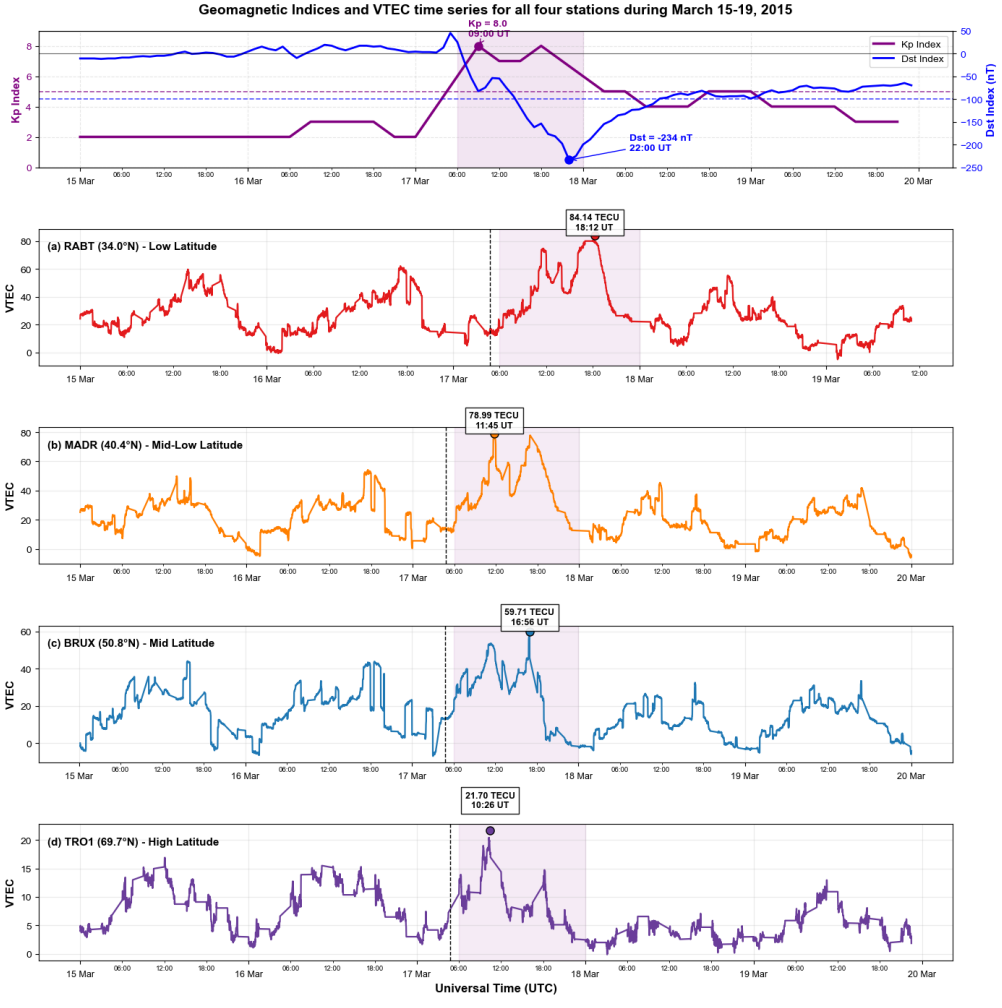

Figure 4. Temporal evolution of geomagnetic indices and VTEC during 15–19 March 2015. The upper panel shows the Kp (purple) and Dst (blue) indices, with the storm main phase shaded. Panels (a)–(d) show the VTEC time series for RABT, MADR, BRUX, and TRO1, respectively. Annotated values indicate the maximum observed VTEC during the study period and are shown for descriptive purposes only; the quantitative inter-station comparison presented later is based on peak hourly mean VTEC values.

https://doi.org/10.5194/egusphere-2026-2994
Preprint. Discussion started: 17 June 2026
© Author(s) 2026. CC BY 4.0 License.

The VTEC time series and hourly mean variations both show stronger daytime ionization at RABT, MADR, and BRUX than at TRO1, reflecting the expected decrease in ionospheric electron content with increasing latitude.

A pronounced storm-time response is observed on 17 March at RABT, MADR, and BRUX. In the VTEC time series (Fig. 4), the maximum observed VTEC reaches 84.1 TECU at RABT, 79.0 TECU at MADR, and 59.7 TECU at BRUX during the storm main phase. In contrast, TRO1 exhibits a weaker and more variable response, with a maximum observed VTEC of 21.7 TECU. These time series indicate a stronger positive storm-time response at the mid-latitude stations than at auroral latitude.

For a more consistent inter-station comparison, hourly mean VTEC variations are shown in Fig. 5 and are used in the subsequent quantitative analysis. At RABT, MADR, and BRUX, the storm day is characterised by a clear daytime enhancement relative to quiet and pre-storm conditions, whereas TRO1 shows a weaker amplitude increase and stronger short-timescale variability.

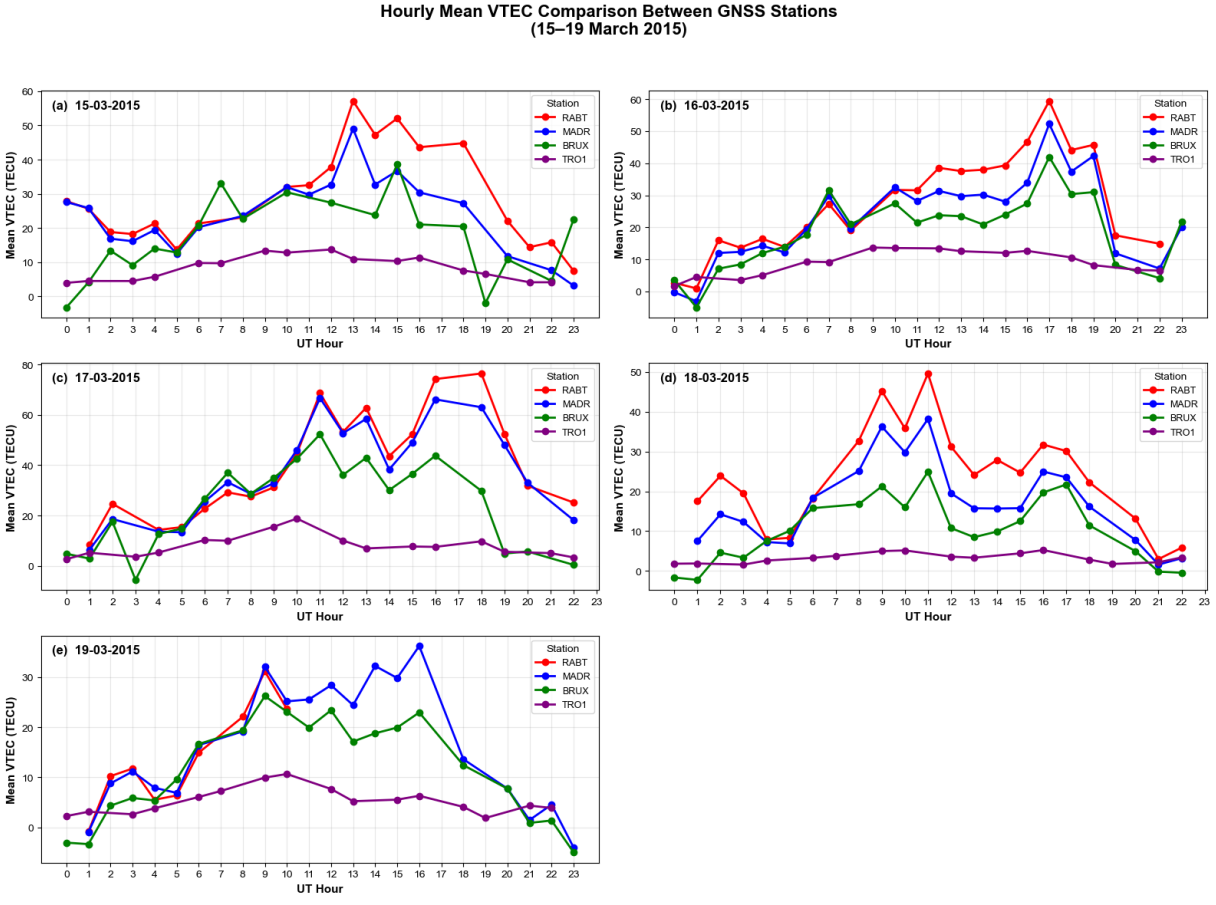

Figure 5. Hourly mean VTEC variations for RABT, MADR, BRUX, and TRO1 during 15–19 March 2015. Different colours indicate individual days, highlighting storm–time departures from quiet–day diurnal behaviour.

https://doi.org/10.5194/egusphere-2026-2994
Preprint. Discussion started: 17 June 2026
© Author(s) 2026. CC BY 4.0 License.

4.3 Storm-time VTEC enhancements and latitudinal gradient

Storm-time VTEC enhancements relative to the quiet-day hourly baseline are summarised in Table 3.

Table 3. Storm-time VTEC enhancements at all stations.

Station	Baseline at peak hour (TECU)	Peak hourly (TECU)	Peak Time (UTC)	Peak Date	Enhancement (%)
RABT	43.8	76.4	18:00	17 Mar	+75
MADR	29.6	66.6	11:00	17 Mar	+125
BRUX	16.2	52.3	11:00	17 Mar	+224
TRO1	12.9	18.8	10:00	17 Mar	+46

Baseline values correspond to the quiet-day hourly baseline evaluated at the UTC hour of the storm-time peak. Peak VTEC represents the peak hourly mean VTEC. Enhancement is calculated as $(\mathrm{Peak} - \mathrm{Baseline})/\mathrm{Baseline} \times 100\%$.

The largest relative enhancement is observed at BRUX (+224%), followed by MADR (+125%), RABT (+75%), and TRO1 (+46%). All peak hourly mean VTEC values occur on 17 March, indicating a stronger positive storm-time response at the mid-latitude stations than at high latitude. The latitudinal dependence of peak storm-time VTEC is shown in Fig. 6.

Peak VTEC decreases systematically with increasing latitude, with a linear regression yielding a negative gradient of -1.61 ± 0.06 TECU per degree ($R^2 = 0.9968$, $p = 0.001578$). This trend indicates that the absolute storm-time VTEC peak decreases systematically with latitude across the station transect, whereas relative enhancements depend additionally on the quiet-day baseline at each station, with the auroral station exhibiting a more limited storm–time enhancement. The gradient reported here should therefore be viewed as a first-order sectorial estimate, while its generality should be tested using denser station coverage in future work. The particularly large relative enhancement observed at BRUX should be interpreted in light of both storm-time forcing and the station-dependent quiet-day baseline. Although BRUX does not exhibit the largest absolute peak VTEC, its lower baseline at the time of peak leads to a stronger relative enhancement, illustrating that percentage increases do not map directly onto absolute storm-time amplitudes.

https://doi.org/10.5194/egusphere-2026-2994
Preprint. Discussion started: 17 June 2026
© Author(s) 2026. CC BY 4.0 License.

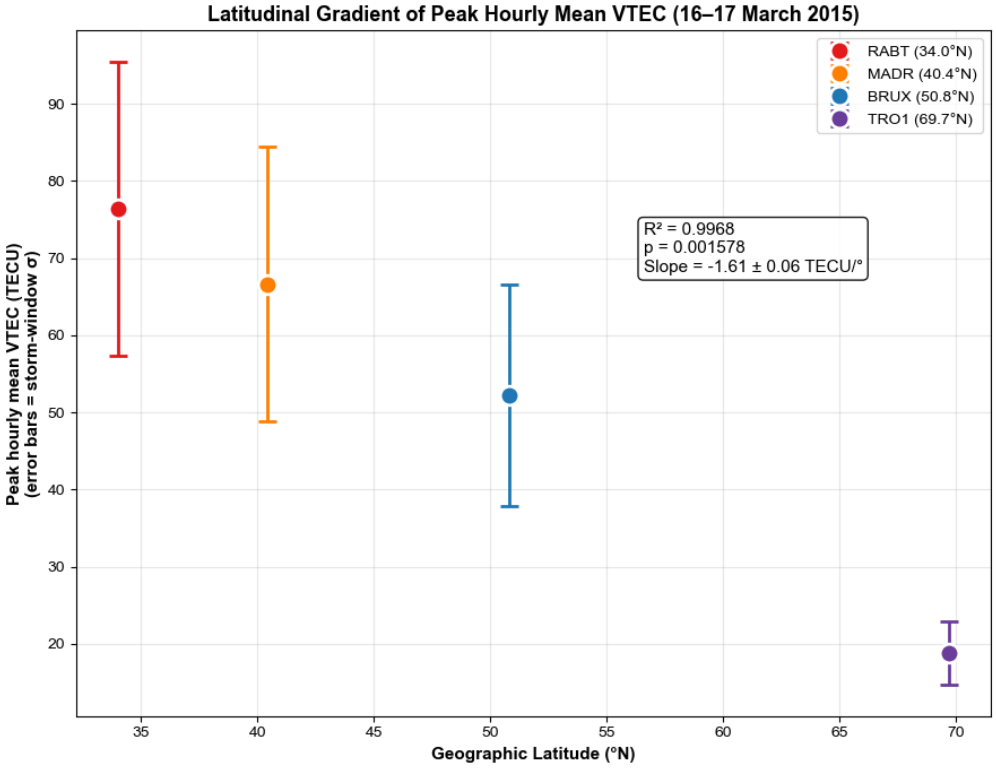

Figure 6. Latitudinal dependence of peak storm-time VTEC. Linear regression shows a systematic decrease in peak hourly mean VTEC with latitude ($R^2 = 0.9968$, $p = 0.001578$). Error bars represent the standard deviation of hourly VTEC within the selected storm-time analysis window.

4.4 Correlation analysis

To quantify the relationship between ionospheric TEC variability and geomagnetic activity, we computed Pearson correlation coefficients between hourly ΔVTEC and Kp, as well as between hourly ΔVTEC and $-\mathrm{Dst}$, for all stations. The results are summarised in Fig. 7 and Table 4.

Previous work has linked ionospheric TEC variability to geomagnetic activity, particularly through K-index-based diagnostics (Nebdi et al., 2004). In the present analysis, the clearest association is found between ΔVTEC and Kp at RABT and MADR, where statistically significant positive correlations are observed. BRUX shows a weaker positive correlation, while TRO1 shows a weak negative correlation. By contrast, correlations between ΔVTEC and $-\mathrm{Dst}$ remain weak at all stations.

https://doi.org/10.5194/egusphere-2026-2994
Preprint. Discussion started: 17 June 2026
© Author(s) 2026. CC BY 4.0 License.

Table 4. Pearson correlation coefficients between ΔVTEC and geomagnetic indices.

Station	$r(\Delta\mathrm{VTEC}, \mathrm{Kp})$	$p(\mathrm{Kp})$	$r(\Delta\mathrm{VTEC}, -\mathrm{Dst})$	$p(-\mathrm{Dst})$
RABT	0.333	0.0014	0.172	0.2419
MADR	0.375	0.0001	0.155	0.2414
BRUX	0.238	0.0151	-0.097	0.4509
TRO1	-0.140	0.2151	-0.110	0.4557

Correlations were computed using paired hourly ΔVTEC and geomagnetic-index values. Following the significance criterion adopted in Sect. 3.5, only correlations with $p < 0.01$ are considered statistically significant.

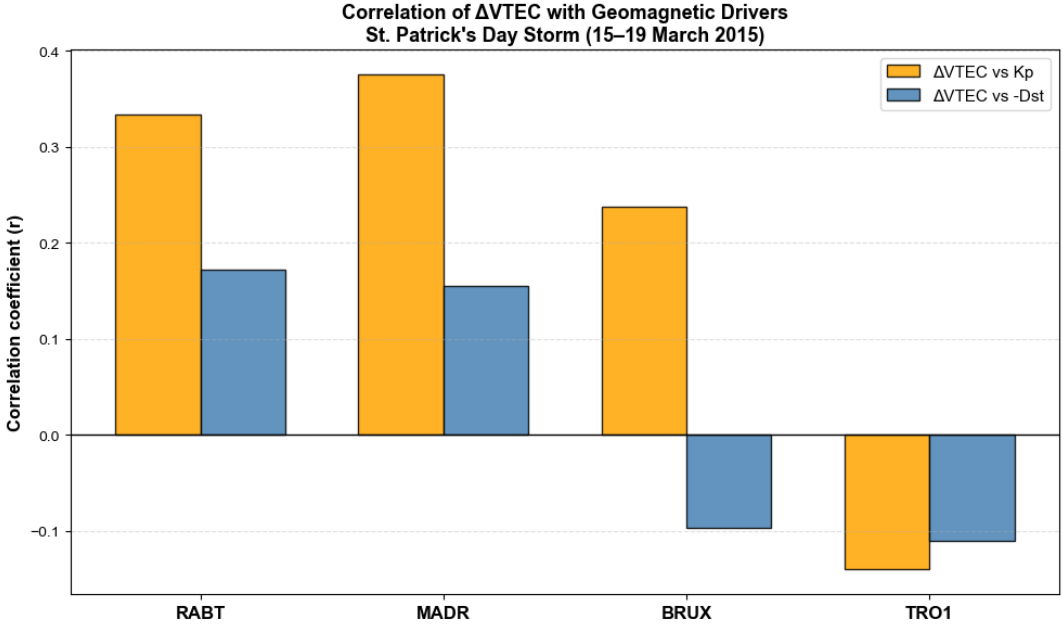

Figure 7. Correlation of ΔVTEC with geomagnetic indices for all stations during 15–19 March 2015. Orange bars: $r(\Delta\mathrm{VTEC}, \mathrm{Kp})$; blue bars: $r(\Delta\mathrm{VTEC}, -\mathrm{Dst})$. Moderate positive correlations with Kp are observed at RABT and MADR, while BRUX shows a weaker positive correlation that is not statistically significant under the adopted $p < 0.01$ criterion. Correlations with $-\mathrm{Dst}$ remain weak at all stations.

4.4.1 Kp correlations

The ΔVTEC–Kp relationship shows the clearest coupling with geomagnetic activity among the two indices considered (Figure 8). The strongest positive correlation is observed at MADR ($r = 0.375$), followed by RABT ($r = 0.333$). BRUX also exhibits a weaker positive correlation ($r = 0.238$), whereas TRO1 shows a weak negative correlation ($r = -0.140$).

These results indicate that the storm-time ionospheric response is more closely related to Kp at the mid-latitude stations than at high latitude. The relatively stronger response at MADR and RABT is consistent with more effective coupling between geomagnetic activity and positive storm-time TEC perturbations at these latitudes. In contrast, the weaker relationship at TRO1

https://doi.org/10.5194/egusphere-2026-2994
Preprint. Discussion started: 17 June 2026
© Author(s) 2026. CC BY 4.0 License.

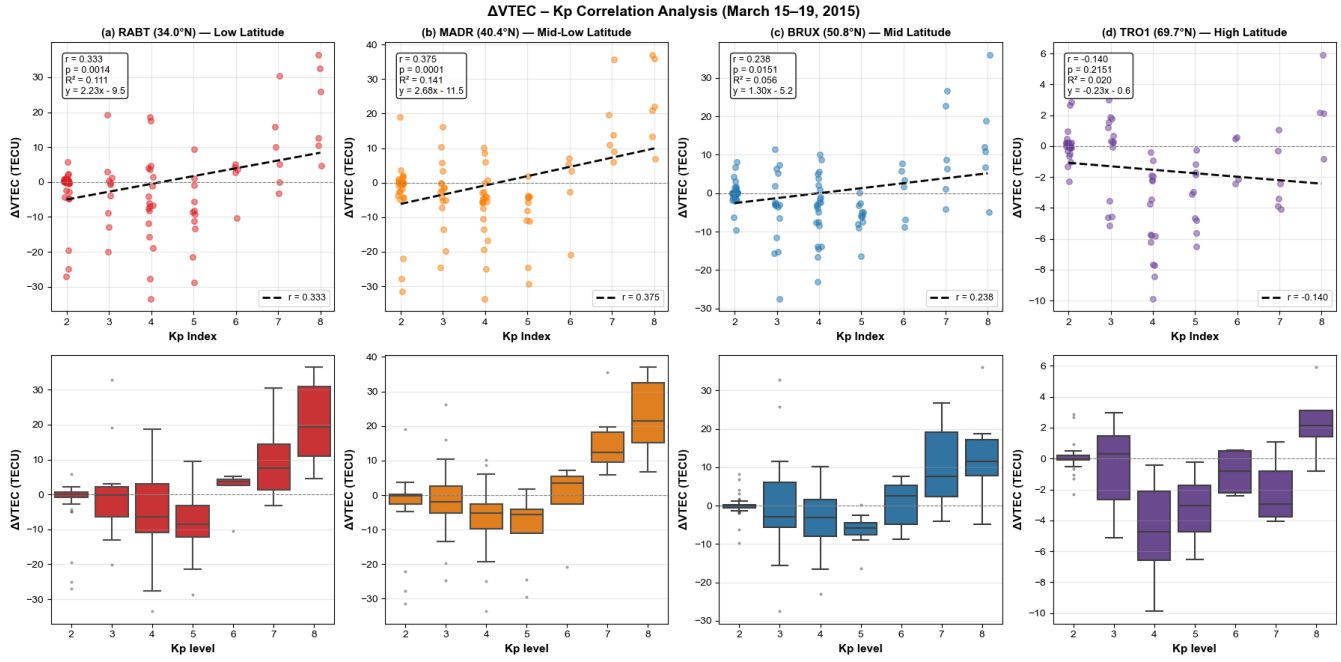

Figure 8. Scatter plots and box plots of ΔVTEC versus Kp index for all four stations during 15–19 March 2015. Top panels show scatter plots with linear regression (black dashed lines). Bottom panels show box plots grouped by Kp level, illustrating stronger positive storm-time responses at RABT and MADR and weaker trends at BRUX and TRO1.

suggests that auroral-zone ionospheric variability is influenced by more localized and variable forcing mechanisms, including particle precipitation, electrodynamic forcing, and composition changes, which are not fully captured by a simple linear relation with Kp (Nava et al., 2016).

The stronger ΔVTEC–Kp correlation at MADR compared with RABT suggests that MADR may occupy a favourable latitude range for storm-time coupling between geomagnetic activity and ionospheric TEC enhancement. At this latitude, prompt penetration electric fields may still contribute efficiently to plasma uplift, while the competing effects that become more important at higher latitudes remain less dominant. This may allow TEC variability at MADR to respond more directly to global geomagnetic activity than at TRO1, where local auroral processes introduce greater variability. The moderate rather than strong correlation levels obtained with Kp likely reflect the combined influence of several factors that are not captured by a simple linear relationship. These include local-time dependence, latitude-dependent electrodynamics, partial saturation of Kp during intense activity, and the coexistence of multiple storm-time mechanisms such as PPEFs, DDEFs, and composition-driven effects. As a result, Kp captures part of the storm forcing, but not the full complexity of the regional TEC response.

4.4.2 Correlations with −Dst

The ΔVTEC with −Dst relationship is weaker than the corresponding ΔVTEC–Kp relationship (Fig. 9).

https://doi.org/10.5194/egusphere-2026-2994
Preprint. Discussion started: 17 June 2026
© Author(s) 2026. CC BY 4.0 License.

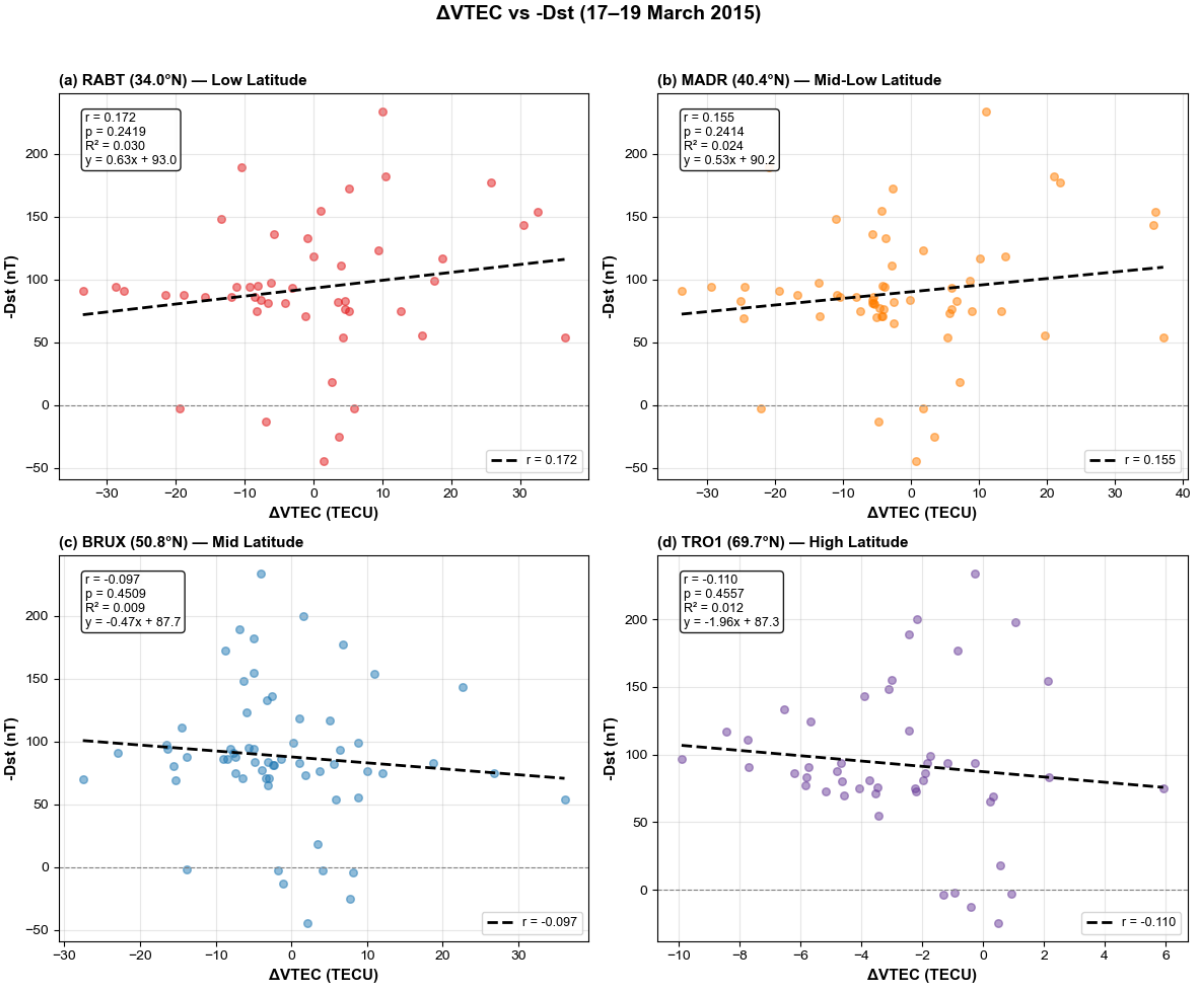

Figure 9. Scatter plots showing the relationship between hourly ΔVTEC and −Dst for RABT, MADR, BRUX, and TRO1 during 17–19 March 2015. Dashed lines indicate linear regression fits, and the corresponding correlation statistics are shown in each panel.

https://doi.org/10.5194/egusphere-2026-2994
Preprint. Discussion started: 17 June 2026
© Author(s) 2026. CC BY 4.0 License.

Weak positive correlations are found at RABT ($r = 0.172$) and MADR ($r = 0.155$), whereas BRUX ($r = -0.097$) and TRO1 ($r = -0.110$) show weak negative correlations. Overall, the correlation magnitudes remain small, and the associated p-values are large, indicating that no statistically significant linear relationship is found between ΔVTEC and $-\mathrm{Dst}$ for this event. The negative tendency observed at the higher-latitude stations may be consistent with the increasing influence of composition changes, enhanced recombination, and, at the highest latitudes, auroral forcing, all of which can reduce ionospheric electron density during disturbed conditions (Prölss, 1995; Burns et al., 2004). These results suggest that, within the present dataset, $-\mathrm{Dst}$ is less effective than Kp in capturing the station-to-station variability of storm-time TEC perturbations. This weaker relationship likely reflects the fact that Dst primarily describes the intensity of the ring current, whereas ionospheric TEC variability in the European–African sector is additionally influenced by local time, latitude-dependent electrodynamics, thermospheric composition changes, and, particularly at auroral latitude, particle precipitation and auroral energy input. Consequently, although Dst remains useful as a measure of storm intensity, it does not show a strong direct linear correspondence with ΔVTEC in the present analysis.

4.5 Time-lagged response analysis

To quantify the temporal coupling between geomagnetic activity and ionospheric response, a time-lagged cross-correlation analysis was performed between hourly ΔVTEC and the Kp index using time lags ranging from -12 to $+12$ hours (Figure 10). Prior to the cross-correlation computation, both ΔVTEC and Kp were high-pass filtered using a 24-hour centred rolling mean subtraction to remove slow recovery trends and isolate storm-time variability. The dashed lines in Figure 10 indicate the approximate significance level $\pm 1.96/\sqrt{n}$, shown as a visual reference; this criterion assumes independent observations and should therefore be interpreted as indicative rather than as a formal statistical threshold.

RABT and MADR exhibit maximum correlations at short positive lags of approximately $+1$ hour, whereas BRUX reaches its maximum correlation at approximately $+2$ hours. These short delays indicate that the strongest storm-time ionospheric response at these stations occurs shortly after enhanced geomagnetic activity. Among them, BRUX shows the highest maximum correlation, followed by MADR and RABT. These short delays are consistent with a rapid ionospheric adjustment to storm-time forcing across the mid-latitude sector.

In contrast, TRO1 exhibits its maximum correlation at approximately $\tau \approx 0$ hours, suggesting a near-simultaneous response with respect to Kp variations. This behaviour indicates that, at auroral latitude, ionospheric variability is more immediate and likely influenced by localized high-latitude forcing processes acting on shorter timescales.

At TRO1, the weaker and partly negative coupling with geomagnetic indices is consistent with the growing influence of auroral-zone forcing, including particle precipitation, composition changes, and enhanced recombination. These processes can reduce or strongly modulate local electron density, even during intense geomagnetic activity. An additional factor that likely contributes to the station-to-station differences in storm-time response is local time. Although MADR and BRUX reach their peak hourly mean VTEC around 11:00 UTC, RABT peaks later, at 18:00 UTC. Because these stations occupy different longitudes and local electrodynamic conditions, the same geomagnetic forcing does not necessarily produce maximum TEC enhancement at the same universal time. In particular, the later response at RABT may reflect the role of afternoon-sector

https://doi.org/10.5194/egusphere-2026-2994
Preprint. Discussion started: 17 June 2026
© Author(s) 2026. CC BY 4.0 License.

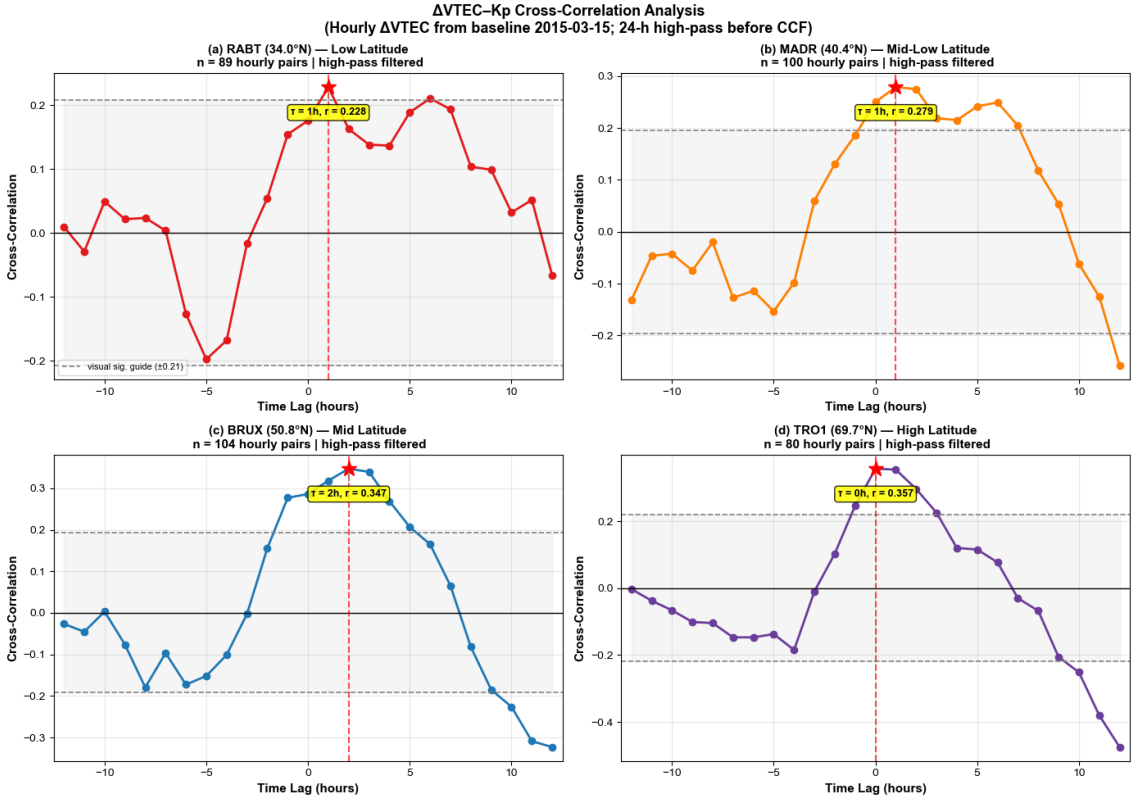

Figure 10. Time-lagged cross-correlation between hourly ΔVTEC and Kp for the four stations after 24-hour high-pass filtering of both series. The optimal lag corresponds to the lag at which the maximum cross-correlation coefficient is obtained. Positive lag values indicate that the ionospheric response follows the geomagnetic forcing. Dashed lines indicate the approximate visual significance guide $\pm 1.96/\sqrt{n}$.

ionospheric conditions, under which storm-time uplift and plasma redistribution can evolve differently from the responses observed earlier over Europe.

Overall, the time-lagged analysis indicates that the storm-time ionospheric response occurs within a few hours of enhanced geomagnetic activity across the study sector, with short positive delays at RABT, MADR, and BRUX and an approximately synchronous response at TRO1. These results support a rapid coupling between geomagnetic activity and ionospheric TEC variability during the 17 March 2015 storm. A limitation of the present analysis is that the latitudinal gradient is derived from four stations only. Although these stations provide a coherent transect from mid- to auroral latitudes and yield a remarkably consistent linear trend, the robustness of the fitted gradient would benefit from future extension to additional intermediate latitudes and complementary GIM-based sampling. A limitation of the present STEC-to-VTEC conversion is the use of a fixed single-layer ionospheric height of 350 km. During strong geomagnetic storms, the effective height of the F-region peak can vary substantially, which may introduce additional uncertainty into the mapping function and thus into the derived VTEC values.

https://doi.org/10.5194/egusphere-2026-2994
Preprint. Discussion started: 17 June 2026
© Author(s) 2026. CC BY 4.0 License.

5 Conclusions

This study investigated the latitude-dependent ionospheric response to the St. Patrick's Day geomagnetic storm of 17 March 2015 using GNSS-derived vertical total electron content (VTEC) from four stations spanning mid- to auroral latitudes in the European–African sector. By combining multi-station GNSS observations with validation against CODE Global Ionosphere Maps, correlation analysis, and time-lagged analysis, this work provides a sector-specific assessment of storm-time ionospheric variability.

The results show a clear latitudinal structuring of the storm-time ionospheric response. Peak storm-time VTEC decreases systematically with increasing latitude, with a linear gradient of -1.61 ± 0.06 TECU per degree. Relative enhancements vary markedly across the station transect, with the largest increase observed at BRUX and the weakest response at TRO1, indicating that storm-time TEC perturbations are strongly latitude dependent in the European–African sector.

Correlation analysis further shows that Kp provides the clearest geomagnetic association with ΔVTEC in the present dataset. Moderate positive correlations are found at RABT and MADR, with a weaker positive response at BRUX, whereas correlations with $-\mathrm{Dst}$ remain weak at all stations. These results suggest that, for this event, Kp is more effective than $-\mathrm{Dst}$ in capturing the station-to-station variability of storm-time TEC perturbations.

Time-lagged cross-correlation analysis indicates that the ionospheric response occurs within a few hours of enhanced geomagnetic activity across the study sector. RABT and MADR exhibit short positive delays of about $+1$ hour, BRUX shows a delay of about $+2$ hours, and TRO1 exhibits an approximately synchronous response. These results support rapid storm-time coupling between geomagnetic activity and ionospheric TEC variability, while also highlighting differences between mid-latitude and auroral-latitude behaviour.

Although the present analysis focuses primarily on the main storm phase, the post-storm period on 18–19 March suggests that recovery-phase behaviour may remain station dependent. A dedicated analysis of recovery-phase ionospheric variability lies beyond the scope of the present paper, but represents an important extension for future work.

Overall, the present analysis shows that ionospheric storm responses in the European–African sector cannot be adequately characterized using single-station observations alone. The combined use of multi-station GNSS measurements, quiet-day baseline removal, correlation analysis, and time-lag assessment provides a more robust framework for resolving the spatial and temporal structure of storm-time TEC variability.

From an applied perspective, these results contribute to regional space weather assessment by quantifying how storm-time VTEC perturbations vary with latitude and geomagnetic forcing. Future work should extend this approach to multiple geomagnetic storms, additional longitude sectors, and coupled physics-based modelling in order to assess the generality of the observed relationships and improve predictive capability.

Code availability. No standalone software package or model code was developed for this study. Data processing and statistical analyses were performed using Python scripts based on standard numerical routines. The scripts are available from the corresponding author upon reasonable request.

https://doi.org/10.5194/egusphere-2026-2994
Preprint. Discussion started: 17 June 2026
© Author(s) 2026. CC BY 4.0 License.

Data availability. The GNSS observation and navigation data used in this study are publicly available from the International GNSS Service archive through the UNAVCO/EarthScope archive (https://www.unavco.org, last access: 17 May 2026). CODE Global Ionosphere Maps and differential code bias products are available from the Center for Orbit Determination in Europe (ftp://ftp.aiub.unibe.ch/CODE/, last access: 17 May 2026). The Kp index is available from the GFZ Helmholtz Centre for Geosciences (https://kp.gfz.de/, last access: 17 May 2026), and the Dst index is available from the World Data Center for Geomagnetism, Kyoto (https://wdc.kugi.kyoto-u.ac.jp/, last access: 17 May 2026).

Author contributions. N.B. conceived the study, developed the data processing methodology, performed all analyses, and prepared the manuscript. T.M. contributed to the interpretation of results and manuscript revision. H.N. supervised the research and contributed to the scientific discussion and manuscript revision. All authors reviewed and approved the final manuscript.

Competing interests. The authors declare that they have no conflict of interest.

Acknowledgements. The authors acknowledge the International GNSS Service (IGS) for providing the GNSS observation and navigation data used in this study. We thank the Center for Orbit Determination in Europe (CODE) for the Global Ionosphere Maps (GIMs) and differential code bias (DCB) products. The Kp index was obtained from the GFZ Helmholtz Centre for Geosciences, and the Dst index was provided by the World Data Center for Geomagnetism, Kyoto. The authors also acknowledge the data access services that facilitated the retrieval of these products through the UNAVCO archive. The authors used AI-assisted language-editing tools to improve clarity and readability. The scientific analysis, results, interpretations, and final manuscript remain the authors' responsibility.

https://doi.org/10.5194/egusphere-2026-2994
Preprint. Discussion started: 17 June 2026
© Author(s) 2026. CC BY 4.0 License.

References

Akala, A. O., Afolabi, R. O., and Otsuka, Y.: Responses of the African-European equatorial-, low-, mid-, and high-latitude ionosphere to geomagnetic storms of 2013, 2015 St. Patrick's Days, 1 June 2013, and 7 October 2015, Adv. Space Res., 72, 775–789, https://doi.org/10.1016/j.asr.2022.10.029, 2023.

Astafyeva, E., Zakharenkova, I., and Förster, M.: Ionospheric response to the 2015 St. Patrick's Day storm: a global multi-instrumental overview, J. Geophys. Res. Space Phys., 120, 9023–9037, https://doi.org/10.1002/2015JA021629, 2015.

Astafyeva, E., Zakharenkova, I., Huba, J. D., Doornbos, E., and van den IJssel, J.: Global ionospheric and thermospheric effects of the June 2015 geomagnetic disturbances: multi-instrumental observations and modelling, J. Geophys. Res. Space Phys., 122, 11 976–11 997, https://doi.org/10.1002/2017ja024174, 2017.

Berényi, K. A., Heilig, B., Urbář, J., Kouba, D., Kis, Á., and Barta, V.: Comprehensive analysis of the ionospheric response to the largest geomagnetic storms from solar cycle 24 over Europe, Front. Astron. Space Sci., 10, 1092850, https://doi.org/10.3389/fspas.2023.1092850, 2023.

Blanc, M. and Richmond, A. D.: The ionospheric disturbance dynamo, J. Geophys. Res., 85, 1669–1686, https://doi.org/10.1029/JA085iA04p01669, 1980.

Borries, C., Mahrous, A. M., Ellahouny, N. M., and Badeke, R.: Multiple ionospheric perturbations during the St. Patrick's Day storm 2015 in the European–African sector, J. Geophys. Res. Space Phys., 121, 11 333–11 349, https://doi.org/10.1002/2016JA023178, 2016.

Buonsanto, M. J.: Ionospheric storms – a review, Space Sci. Rev., 88, 563–601, https://doi.org/10.1023/A:1005107532319, 1999.

Burns, A. G., Wang, W., Killeen, T. L., and Solomon, S. C.: A "tongue" of neutral composition, J. Atmos. Sol.-Terr. Phys., 66, 1457–1468, https://doi.org/10.1016/j.jastp.2004.04.009, 2004.

Chafik, B., El Malki, M., Miskane, F., and Nebdi, H.: Prediction of geomagnetic K-index using machine learning, Int. J. Tech. Phys. Probl. Eng., 16, 331–338, 2024.

Chafik, B., El Malki, M., Miskane, F., and Nebdi, H.: Long-term analysis of geomagnetic activity indices, Int. J. Tech. Phys. Probl. Eng., 16, 129–136, 2024.

Cherniak, I. and Zakharenkova, I.: First observations of super plasma bubbles in Europe, Geophys. Res. Lett., 43, 11 137–11 145, https://doi.org/10.1002/2016GL071421, 2016.

Fejer, B. G. and Scherliess, L.: Empirical models of storm time equatorial zonal electric fields, J. Geophys. Res., 102, 24 047–24 056, https://doi.org/10.1029/97JA02164, 1997.

Habyarimana, V., Habarulema, J. B., and Dugassa, T.: Analysis of ionospheric storm-time effects over the East African sector during the 17 March 2013 and 2015 geomagnetic storms, Earth Planets Space, 75, 58, https://doi.org/10.1186/s40623-023-01812-9, 2023.

Hernández-Pajares, M., Juan, J. M., Sanz, J., Orus, R., Garcia-Rigo, A., Feltens, J., Komjathy, A., Schaer, S. C., and Krankowski, A.: The IGS VTEC maps: a reliable source of ionospheric information since 1998, J. Geod., 83, 263–275, https://doi.org/10.1007/s00190-008-0266-1, 2009.

Hofmann-Wellenhof, B., Lichtenegger, H., and Collins, J.: Global Positioning System: Theory and Practice, Springer-Verlag, Wien–New York, 1992.

Huang, C.-S., Foster, J. C., and Kelley, M. C.: Long-duration penetration of the interplanetary electric field to the low-latitude ionosphere during the main phase of magnetic storms, J. Geophys. Res., 110, A11309, https://doi.org/10.1029/2005JA011202, 2005.

https://doi.org/10.5194/egusphere-2026-2994
Preprint. Discussion started: 17 June 2026
© Author(s) 2026. CC BY 4.0 License.

Jacobsen, K. S. and Andalsvik, Y. L.: Overview of the 2015 St. Patrick's Day storm and its consequences for RTK and PPP positioning in Norway, J. Space Weather Space Clim., 6, A9, https://doi.org/10.1051/swsc/2016004, 2016.

Jodogne, J.-C., Nebdi, H., and Warnant, R.: GPS TEC and ITEC compared with ionosonde data during the Halloween storm, Adv. Radio Sci., 2, 269–273, https://doi.org/10.5194/ars-2-269-2004, 2004.

Kelley, M. C.: The Earth's Ionosphere: Plasma Physics and Electrodynamics, 2nd edn., Academic Press, Burlington, MA, 2009.

Mošna, Z., Barta, V., Berényi, K. A., Mielich, J., Verhulst, T., Kouba, D., Urbář, J., Chum, J., Koucká Knížová, P., Marew, H., Podolská, K., and Bojilova, R.: The March and April 2023 ionospheric storms over Europe, Front. Astron. Space Sci., 11, 1462160, https://doi.org/10.3389/fspas.2024.1462160, 2024.

Nava, B., Rodríguez-Zuluaga, J., Alazo-Cuartas, K., Kashcheyev, A., Migoya-Orué, Y., Radicella, S. M., Amory-Mazaudier, C., and Fleury, R.: Middle- and low-latitude ionosphere response to 2015 St. Patrick's Day geomagnetic storm, J. Geophys. Res. Space Phys., 121, 3421–3438, https://doi.org/10.1002/2015JA022299, 2016.

Navstar GPS Joint Program Office: Navstar GPS Space Segment/Navigation User Interfaces, Interface Control Document ICD-GPS-200, 2000.

Nebdi, H., Warnant, R., and Lejeune, S.: Monitoring ionospheric activity using GPS: the ESA Space Weather Pilot Project, Technical Report of Work Package 222, Solar Influences Data Centre Space Weather Pilot Project, ESA contract 16913/03/NL/LvH, 2004.

Nebdi, H.: Study of geomagnetic activity during three solar cycles using a K-index data base, Umm Al-Qura Univ. J. App. Sci., 2, 33–41, 2010.

Paul, A., Kascheyev, A., Rodriguez-Bouza, M., Pathak, K., Ferreira, A. A., Shetti, D., and Yao, J. N.: Latitudinal features of total electron content over the African and European longitude sector following the St. Patrick's Day storm of 2015, Adv. Space Res., 61, 1890–1904, https://doi.org/10.1016/j.asr.2017.09.012, 2018.

Prölss, G. W.: Ionospheric F-region storms, in: Handbook of Atmospheric Electrodynamics, Vol. 2, edited by: Volland, H., CRC Press, Boca Raton, FL, 195–248, 1995.

Schaer, S., Gurtner, W., and Feltens, J.: IONEX: The IONosphere map EXchange format version 1, in: Proceedings of the IGS AC Workshop, Darmstadt, Germany, 9–11 February 1998, 233–247, 1998.

Schaer, S.: Mapping and predicting the Earth's ionosphere using the Global Positioning System, Ph.D. thesis, University of Bern, Bern, Switzerland, https://doi.org/10.7892/boris.75985, 1999.

Warnant, R., Nebdi, H., and Pottiaux, E.: Near real-time validation of GPS-TEC using ionosonde TEC at Dourbes, Technical Report of Work Package 212, Solar Influences Data Centre Space Weather Pilot Project, ESA contract 16913/03/NL/LvH, 2003.

Wu, C.-C., Liou, K., Lepping, R. P., Hutting, L., Plunkett, S., Howard, R. A., and Socker, D.: The first super geomagnetic storm of solar cycle 24: "The St. Patrick's Day event (17 March 2015)", Earth Planets Space, 68, 151, https://doi.org/10.1186/s40623-016-0525-y, 2016.